ChemCatChem

Research Article
doi.org/10.1002/cctc.202401270

Chemistry Europe
European Chemical Societies Publishing

www.chemcatchem.org

Comparative Study of Si–O–Al and Si–O–Si Bond Stability in HZSM-5 Zeolite Under Steam and Hot Liquid Water Environments

Linhai He,[a, b, c] Jing Niu,[a, b] Songyue Han,[a, b, c] Dong Fan,[a, b, c] Wenna Zhang,[a, b, c] Shutao Xu,*[a, b, c] Yingxu Wei,[a, b, c] and Zhongmin Liu[a, b, c]

Understanding the changes in the zeolite framework and catalytic active sites during zeolite-based vapor-phase and aqueous catalytic processes is crucial. Herein, the evolution of framework T atoms (Si and Al) in ammonium hexafluorosilicate (AHFS)-treated HZSM-5 zeolite under steam and hot liquid water (HLW) environments was inverstigated using various characterization techniques. In HLW, Si–O–Si bonds exhibit poorer hydrothermal stability than Si–O–Al bonds, in contrast to steam. Significant Si atom leaching occurs regardless of whether the framework tetrahedral Al atoms (Al(IV)-1) are removed. Similar to steam, Al(IV)-1 species in HLW sequentially evolve into partially coordinated framework Al species and then into extra-framework Al (EFAL) species through partial and complete hydrolysis. The generated EFAL species act as Lewis acid sites, but their local structures or chemical environments may differ. These findings reveal the difference in the T–O–T bonds attacked by water molecules: the Si–O–Al bonds are primarily attacked in steam, whereas the Si–O–Si bond are primarily attacked in HLW.

Introduction

Zeolites, remarkable microporous materials with tunable channel structures, acidity and shape selectivity, have shown unmatched catalytic performance in many vapor-phase petrochemical and oil refining processes,[1] as well as in aqueous biomass conversion and upgrading.[2] Many zeolite-based catalytic processes involve water either as a reactant, product or solvent. Water's state, whether gaseous or condensed, depends on temperature and pressure. The irreversible hydrolysis of framework T–O–T bonds can lead to dealumination and desilication, significantly impacting catalytic performance, including activity, selectivity, and longevity. Therefore, it is crucial to thoroughly investigate the hydrothermal stability of zeolites and the evolution of framework T atoms (Si and Al) in steam and hot liquid water (HLW) environments. Notably, zeolites show different thermal susceptibilities in steam versus HLW.[3] Severe steam environments cause dealumination primarily, resulting in only partial micropore loss and minor microstructural damage.[4] Conversely, in HLW, where the temperature is much lower than in vapor, the instability of zeolites is primarily caused by desilication, leading to rapid structural collapse and a dramatic decrease in crystallinity within a few hours.[5]

Recent studies have focused on the factors affecting the hydrothermal stability of zeolites framework and corresponding strategies to enhance resistance against hydrolytic destruction in both environments.[6] Key approaches include introducing extra-framework phosphorus species, applying surface coatings with hydrophobic materials (e.g., organosilanes, carbon overlayers), using fluoride media during zeolite synthesis, and functionalizing zeolites with organosilanes.[7] Additionally, attention has been given to the dynamic structural evolution of framework tetrahedral Al atoms, Al(IV)-1, which serve as catalytic active sites. Compared to HLW environment, the literature on the dynamic evolution of Al(IV)-1 under steam condition is more comprehensive. In severe steam conditions, Al(IV)-1 species evolve into partially coordinated framework Al, Al(IV)-2, and then into initial $Al(OH)_3{\cdot}H_2O$ EFAL species sequentially through partial and complete hydrolysis.[8] Al(IV)-2 is regarded as a critical intermediate species in the removal of Al atoms from the framework. The initial $Al(OH)_3{\cdot}H_2O$ EFAL species can be further transformed into new forms including cations like Al^{3+}, $Al(OH)^{2+}$, $Al(OH)_2{}^{+}$, AlO^{+} or netural forms like AlO(OH), Al_2O_3 or their clusters like dimers, trimers, serving as Lewis acid sites crucial for zeolite catalytic properties. The Brønsted/Lewis acid synergistic effect[9] between Al(IV)-1 and EFAL, as well as the Brønsted-Brønsted synergistic effect[10] between Al(IV)-1 and Al(IV)-2, both affect catalytic activity. Although zeolite decrystallization under HLW conditions has been extensively studied, understanding the evolution of Al(IV)-1 remains challenging since framework such as FAU and BEA decrystallize at a rapid rate. Lercher et al. found that the local structure of framework Al atoms, including the Al–O–Si angles and bond distances,

[a] L. He, J. Niu, S. Han, D. Fan, W. Zhang, S. Xu, Y. Wei, Z. Liu
National Engineering Research Center of Lower-Carbon Catalysis Technology, Dalian Institute of Chemical Physics, Chinese Academy of Sciences, Dalian 116023, P.R. China
E-mail: xushutao@dicp.ac.cn

[b] L. He, J. Niu, S. Han, D. Fan, W. Zhang, S. Xu, Y. Wei, Z. Liu
State Key Laboratory of Catalysis, Dalian Institute of Chemical Physics, Chinese Academy of Sciences, Dalian 116023, P.R. China

[c] L. He, S. Han, D. Fan, W. Zhang, S. Xu, Y. Wei, Z. Liu
University of Chinese Academy of Sciences, Beijing 100049, P. R. China

Supporting information for this article is available on the WWW under https://doi.org/10.1002/cctc.202401270

remains mostly intact despite the collapse of BEA zeolites after treatment in HLW.[11] In contrast, Maag et al. found that HLW treatment promotes ZSM-5 zeolite dealumination by a mechanism similar to that of steam treatment.[12] Thus, whether there is a difference in the evolution path of framework Al atoms under steam and HLW environments remains unclear. Fortunately, MFI-type zeolites are suitable candidates due to their outstanding hydrothermal stability in both steam and HLW environments.

In this work, a series of HZSM-5 zeolites treated with steam and HLW in an autoclave reactor were obtained. The evolution of the framework T atoms (Si and Al), including the coordination states of Al species, the framework and bulk Si/Al ratio, acid concentration and strength, and the spatial proximity of various hydroxyls, was investigated and compared using a variety of characterization methods.

Results and Discussion

Structural Transformation

Framework-associated Al and EFAL species are inevitably generated during synthesis and calcination to remove the organic structure-directing agent (OSDA). These original Al species may interfere with understanding the true evolution of framework tetrahedral Al species, as they may also be formed after steam and hot liquid water (HLW) treatments. Several studies have demonstrated that chemical washing using ammonium hexafluorosilicate (AHFS) can effectively remove framework-associated Al and EFAL species in zeolites without damaging the framework.[13] Thus, in this study, the prinstine HZSM-5 zeolite was first washed with AHFS to remove framework-associated Al and EFAL species before being treated with steam and HLW. As demonstrated by XRD in Figure S1, the structural integrity of HZSM-5 zeolites remains practically intact following AHFS, steam and HLW treatments. SEM imagines (Figure S2) reveal that the morphology and size of particles exhibit no significant changes following AHFS and steam treatment, with particle sizes ranging from 100 to 400 nm. However, after HLW treatment at 300 °C, particle surfaces appear smoother compared to the AHFS-washed sample, particularly for HZSM-5-AH2. This smoothing, as observed by Vjunov et al., is attributed to the dissolution and reprecipitation of Si atoms within the framework.

To track the dynamic evolution of framework T atoms (Si and Al), ^{27}Al and ^{29}Si MAS NMR experiments were carried out on above HZSM-5 zeolites. ^{27}Al MAS NMR spectra are shown in Figure 1a. After treating with AHFS solution, the peaks around 45 ppm and 0 ppm are completely removed, leaving only the peak around 55 ppm, which is attributed to framework tetrahedral-coordinated Al species (Al(IV)-1). The asymmetry of this peak suggests at least two types of tetrahedrally coordinated Al species. Given that ^{27}Al is a nucleus with S = 5/2, its resolution is constrained by residual second-order quadrupole broadening, which is not entirely eliminated by magic angle spinning. Therefore, ^{27}Al MQ MAS NMR was employed to better

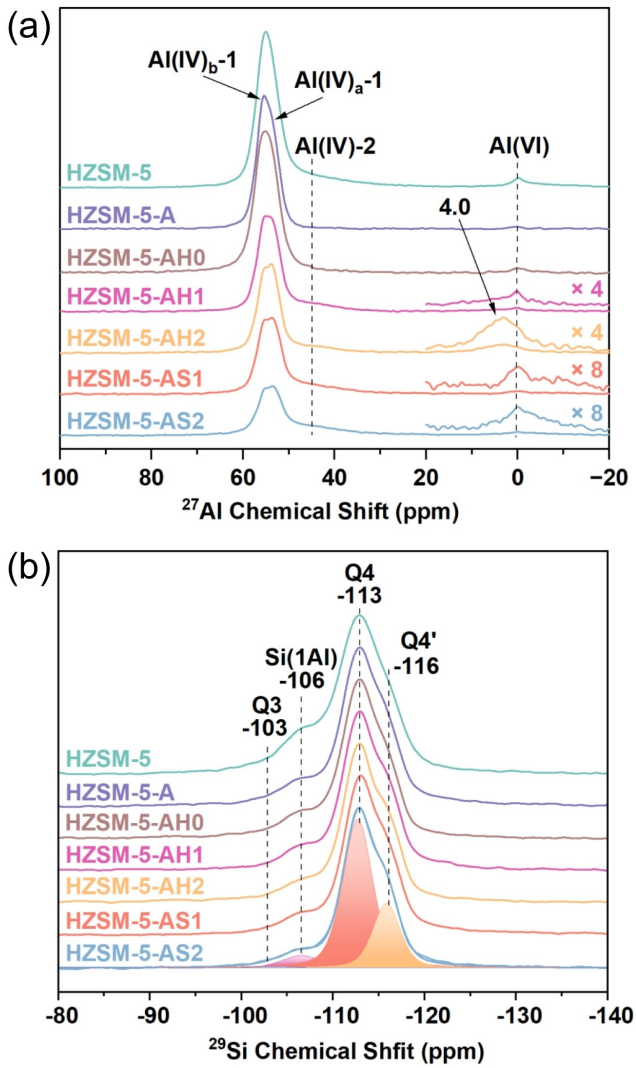

Figure 1. ^{27}Al MAS NMR spectra (a), ^{29}Si MAS NMR spectra (b) of HZSM-5 zeolites before and after AHFS, steam and HLW treatments. Note that the intensities in ^{27}Al MAS NMR spectra have been normalized by mass and all samples are fully hydrated.

differentiate the various Al species. NMR parameters of different Al species extracted from ^{27}Al MQ MAS NMR spectra are listed in Table S1. In the ^{27}Al MQ MAS NMR spectra of HZSM-5-A (Figure 2a), two types of tetrahedrally coordinated Al species, with isotropic chemical shifts of 53.8 ppm (Al(IV)$_a$-1) and 57.2 ppm (Al(IV)$_b$-1), are identified, caused by the different distribution of Al atoms over the 12 distinct T-sites of the MFI structure. For HZSM-5-AH0 sample, only the peak around 55 ppm was still observed, while the intensity of Al(IV)-1 remained almost unchanged, indicating treating with HLW at 200 °C for 12 hours did not cause dealumination. However, treating at 300 °C for 4 hours (HZSM-5-AH1) and 12 hours (HZSM-5-AH2) caused the intensity of Al(IV)-1 to gradually decrease, accompanied by the sequential emergence of peaks around 45 ppm and 4.0 ppm. A similar transformation occurs after steam treatment, but with fewer Al(IV)-1. The new broad peak around 45 ppm in HZSM-5-AH1 (Figure 2b) and HZSM-5-

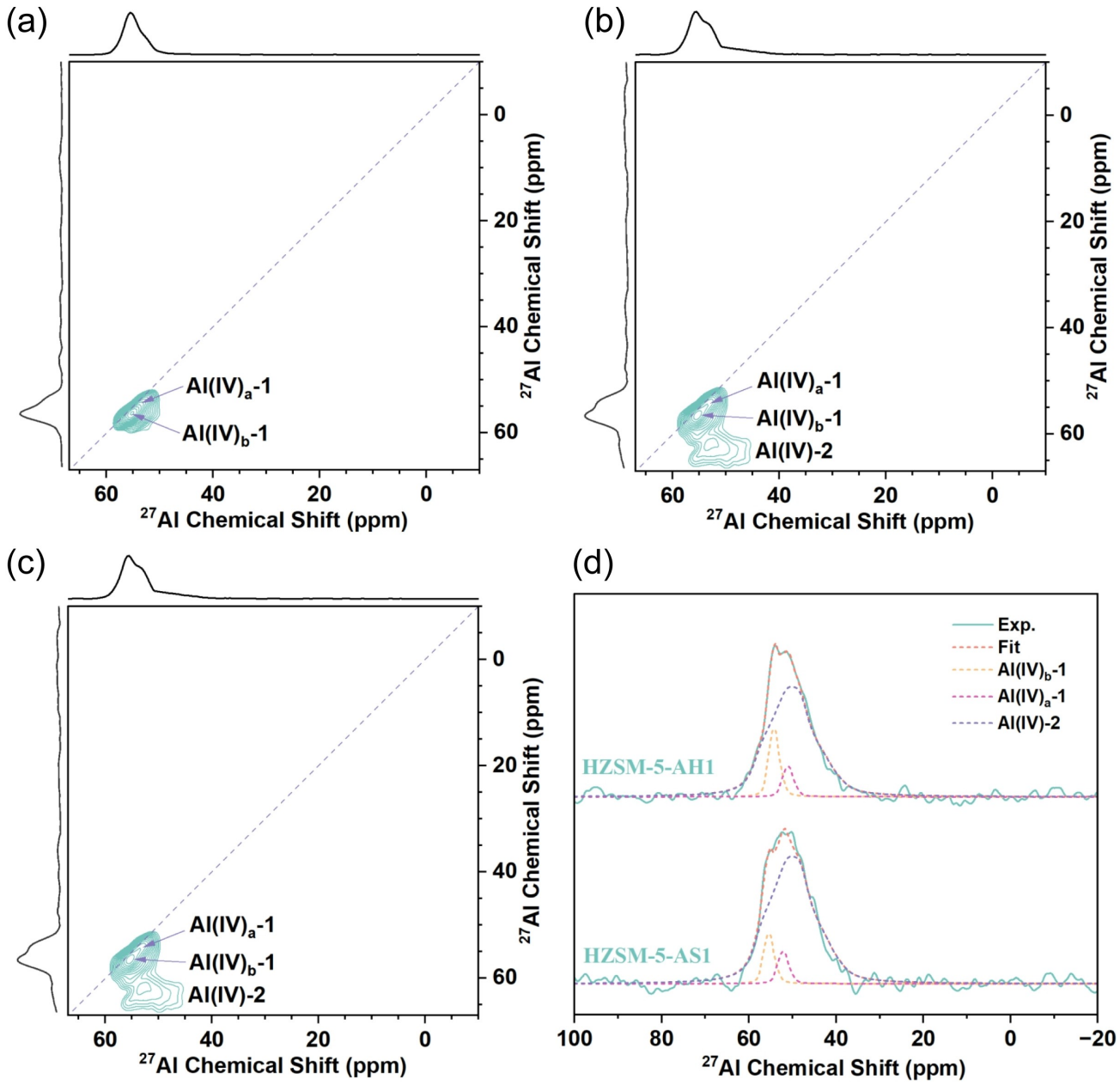

Figure 2. ^{27}Al MQ MAS NMR spectrum of HZSM-5-A (a), HZSM-5-AH1 (b) and HZSM-5-AS1 (c). Deconvolution of 1D projection at F1 = 63.0 ppm in ^{27}Al MQ MAS NMR spectra of HZSM-5-AH1 and HZSM-5-AS1 samples. All samples are fully hydrated.

AS1 (Figure 2c) samples exhibit similar NMR parameters (Table S1), including isotropic chemical shifts (δ_{iso} = 60.2 or 58.9 ppm), an asymmetry factor (η = 0.65), and a large quadrupole coupling constant (C_Q = 5.6 MHz), and is assigned to partially bonded framework $(SiO)_{4-n}$-Al$(OH)_n$ species (Al(IV)-2).[14] Peaks at 4.0 ppm and 0 ppm correspond to octahedral-coordinated Al species (Al(VI)), which may have different local structures or chemical environments.[15]

To determine whether Al(VI) was framework-associated Al or EFAL, the HZSM-5-AH2 sample was converted to the ammonium form. As shown in Figure S3, the irreversible octahedral-to-tetrahedral coordination transformation indicates that the observed Al(VI) can be considered EFAL species rather than framework-associated Al.[16] Notably, the ^{27}Al chemical shift of Al(VI) generated by HLW treatment is shifted to a lower field, appearing at 4.0 ppm instead of 0 ppm, indicative of different local structure or chemical environments. Reintroduction of Al(IV)-2 and Al(VI) species after being exposed to steam and HLW environments indicates the irreversible hydrolysis of framework Si–O–Al bonds. This phenomenon differs from Vjunov's research results that the local structure of framework Al atoms, including the Al–O–Si angles and bond distances, remains mostly intact despite the collapse of BEA zeolites after treatment in HLW, as determined by Al extended X-ray absorption fine structure analysis.[11] As shown in Figure 1a, Al(IV)$_b$-1 was preferentially removed in both HLW and steam

environments compared to Al(IV)$_a$-1, indicating higher lability, consistent with previous studies.[4c,17] The chemical shift of the ^{27}Al MAS NMR spectrum of the MFI-type zeolite shifts to higher magnetic field as the mean T–O–T angle increases, suggesting a lower T–O–T angle for Al(IV)$_b$-1.[18] This higher lability can be rationalized by considering the reduced polarizability at sites with more acute T–O–T angle, making protonation less favorable.[19] Ong et al. proposed that the higher hydrothermal stability of larger T–O–T angle can be explained by their flexibility, which permits distortion of the Al–O bond especially in terms of the resulting angle strain.[17] It is noteworthy that the bulk Si/Al ratio decreases slightly after HLW treatment but remaines essentially unchanged after steam treatment. However, upon mass normalization of the ^{27}Al MAS NMR spectrum, the decrease in intensity of Al(IV)-1 is notably unbalanced by the increase in Al(IV)-1 and Al(VI) species, particularly evident in steam treatment, indicative of the existence of "NMR invisible" Al species with high quadrupole coupling constants.

To gain insight into the local structural environments surrounding Si atoms, ^{29}Si MAS NMR experiments were conducted, as shown in Figure 1b. Peaks at −103 and −106.5 ppm are attributed to Q3 Si(OSi)$_3$(OH) and Si(OSi)$_3$(OAl) species, respectively, while peaks at −113 and −116 ppm are indicative of Q4 Si(OSi)$_4$ species.[20] After washing with AHFS, the intensity of Si(OSi)$_3$(OAl) species decreased significantly due to the removal of Al(IV)-2 and Al(VI) species, increasing the framework Si/Al ratio from 23.2 to 37.7 (Table 1). The intensity of Si(OSi)$_3$(OAl) species remained almost unchanged after treating with HLW at 200 °C for 12 hours. However, both HLW and steam treatments at 300 °C further reduced the intensity of Si(OSi)$_3$(OAl) species, increasing the framework Si/Al ratio, with steam treatment having a more pronounced effect. Moreover, HZSM-5-A zeolite dissolution in HLW was monitored by measuring the concentration of Al and Si in the supernatant using ICP-OES, as listed in Table 1. The results revealed significant Si leaching: 6.81% after treatment at 200 °C for 12 hours, and 7.34% and 11.35% after treatment at 300 °C for 4 and 12 hours, respectively. In contrast, Al dissolution was minimal (< 0.3%). Correspondingly, the bulk Si/Al ratio also decreased from 33.7 to 30.5, 31.3 and 29.3, respectively. Combined with the ^{27}Al MAS NMR results, it is evident that in the HLW environment, desilication occurs exclusively at 200 °C, while both dealumination and desilication occur simultaneously at 300 °C, indicating the poorer hydrothermal stability of the Si–O–Si bond compared to the Si–O–Al bond. Similar desilication in HLW have been observed in other topological zeolites such as Y, beta and ZSM-22.[5] The pKw of water decreases from 14.0 at 25 °C to 11.3 at 200 °C and 11.4 at 300 °C, respectively.[21] This indicates a significantly increased concentration of ionic species (H^+ and OH^-) under the HLW environments studied here.The abundance of H^+ and OH^- in HLW promotes the irreversible hydrolysis of Si–O–Al and Si–O–Si bonds, respeticely, leading to dealumination and significant Si leaching.

The changes in textural properties resulting from steam and HLW treatments were studied through N_2 adsorption-desorption experiments, as shown in Figure S4. All HZSM-5 zeolites exhibited type IV isotherms. The textural properties of these samples are summarized in Table 1. After AHFS washing, the micropore surface area and micropore volume remained nearly unchanged, while the external surface area and mesopore volume increased slightly. In comparison to HLW treatment, steam-treated HZSM-5 zeolites had lower micropore surface area and volume but higher external surface area and mesopore volume. Despite the significantly lower amount of water used in steam treatment (0.4 mL) compared to HLW treatment (40 mL), the degree of damage to the pore structure varied greatly. Figure S5 shows that steam treatment results in smaller pores (2–3 nm), while HLW treatment results in larger pores (10–260 nm). This difference may be attributed to the irreversible hydrolysis of different T–O–T bonds in the two environments: steam primarily induces dealumination through the hydrolysis of Si–O–Al bonds, whereas HLW primarily induces desilication through the hydrolysis of Si–O–Si bonds.

Table 1. Relative crystallinity, chemical compositions and textural properties of HZSM-5 zeolites.

Samples	C_{XRD}[a]	Framework Si/Al[b]	Bulk Si/Al[c]	Dissolved Al (%)[c]	Dissolved Si (%)[c]	S_{BET}[d]	S_{micro}[e]	S_{ext}[f]	V_{total}[g]	V_{micro}[h]	V_{meso}[i]
HZSM-5	100	23.2	15.7	–	–	362	245	117	0.193	0.113	0.080
HZSM-5-A	100	37.7	33.7	–	–	379	241	138	0.204	0.110	0.094
HZSM-5-AH0	107	36.3	30.5	0.22	6.81	373	236	137	0.219	0.108	0.111
HZSM-5-AH1	109	39.0	31.3	0.14	7.34	369	226	143	0.206	0.103	0.103
HZSM-5-AH2	104	44.4	29.3	0.16	11.35	364	212	152	0.193	0.096	0.097
HZSM-5-AS1	107	45.8	32.2	–	–	381	209	172	0.207	0.095	0.112
HZSM-5-AS2	106	55.9	34.1	–	–	371	185	186	0.202	0.083	0.119

[a] Taking the HZSM-5 as a reference, the relative crystallinity (C_{XRD}) was determined by the diffraction peak area ratio of 22.5–25.0 2θ in the XRD spectra. [b] The values of the framework Si/Al ratio were obtained from the formula: $(Si/Al)_{NMR} = \frac{I_4+I_3+I_2+I_1+I_0}{I_4+0.75I_3+0.5I_2+0.25I_1}$, where I_n represents the area of the NMR peak corresponding to the Si(nAl) unit. [c] ICP. [d] BET Method. [e,h] t-plot method. [f] $S_{ext} = S_{BET} - S_{micro}$. [g] $P/P_0 = 0.975$. [i] $V_{meso} = V_{total}$-V_{micro}.

Acidity

The dynamic evolution of hydroxyl groups was elucidated through ^{1}H MAS NMR and FTIR spectroscopy. The concentrations of various hydroxyl groups based on ^{1}H MAS NMR are listed in Table 2. Following AHFS washing, only four peaks at 4.5, 3.9, 2.0 and 1.7 ppm are observed in Figure 3a, indicative of the removal of other hydroxyl groups accompanying the removal of framework-associated Al and EFAL species. Specifically, the peaks at 3.9, 2.0, and 1.7 ppm are attributed to the unperturbed Brønsted acid sites (BASs), geminal or vicinal Si–OH groups, and isolated Si–OH groups, respectively.[22]

Table 2. Concentrations of different hydroxyl groups of HZSM-5 zeolites by quantifying and deconvoluting the ^{1}H MAS NMR spectra, in units of mmol/g.

Samples	12–15 ppm	6–9 ppm	4.6 ppm	3.9 ppm BAS	2.5 ppm Al–OH	1.7–2.0 ppm Si–OH	Sum of all species excluding Si–OH	Total
HZSM-5	0.025	0.093	0.272	0.261	0.108	0.066	0.759	0.825
HZSM-5-A	0	0	0.230	0.163	0	0.052	0.393	0.445
HZSM-5-AH1	0.020	0.012	0.160	0.157	0.054	0.055	0.402	0.457
HZSM-5-AH2	0.015	0	0.151	0.138	0.050	0.048	0.355	0.403
HZSM-5-AS1	0.014	0.060	0.146	0.107	0.060	0.052	0.386	0.439
HZSM-5-AS2	0.023	0.015	0.079	0.105	0.074	0.048	0.295	0.343

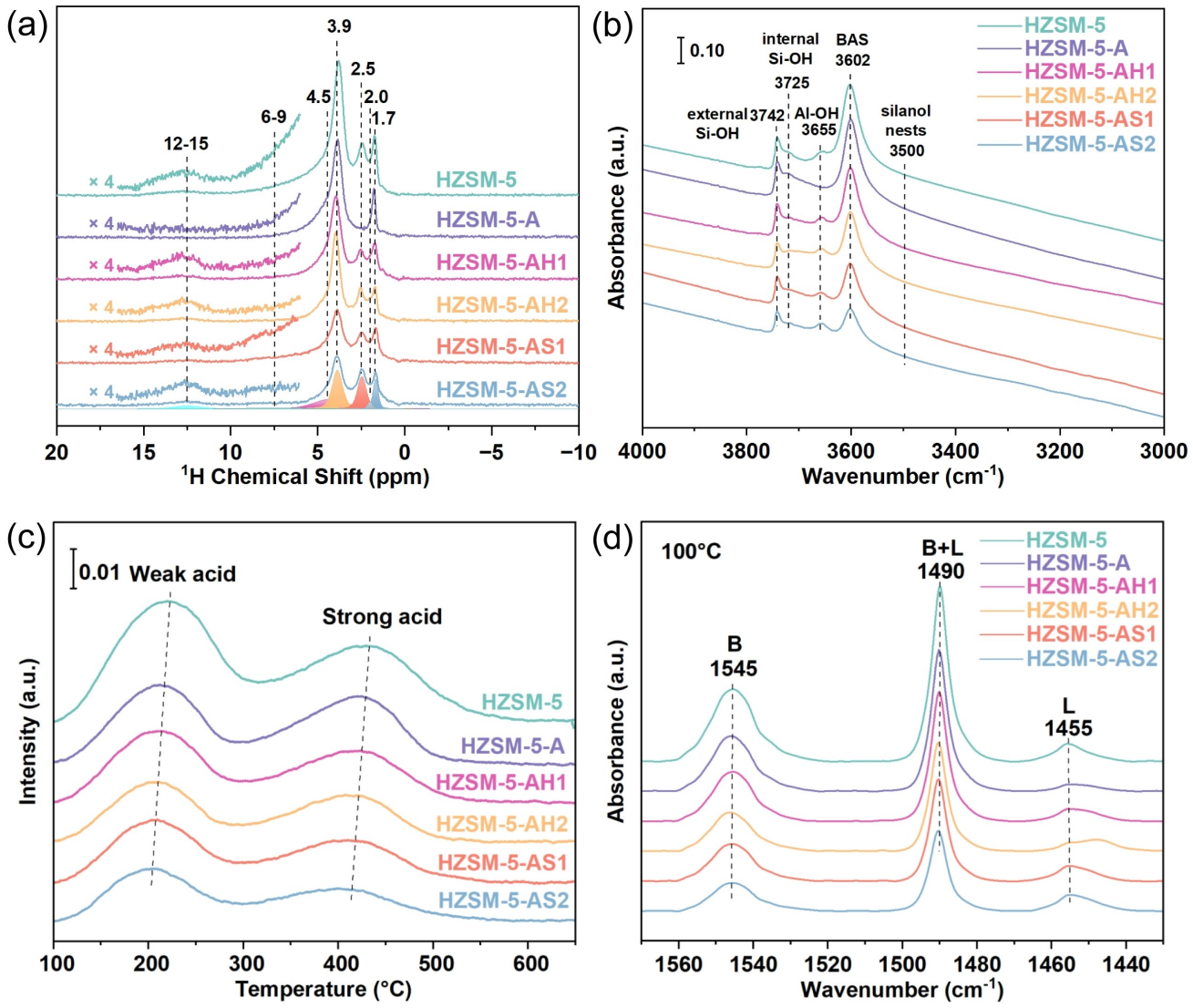

Figure 3. ^{1}H MAS NMR spectra (a), FTIR spectra of the OH vibration region (b), NH_3-TPD profiles (c) and pyridine adsorbed FT-IR spectra at 100 °C (d) of HZSM-5 zeolites before and after AHFS, steam and HLW treatments. Note that the intensities in a-d have been normalized by mass.

However, the precise assignment of the broad shoulder peak at 4.5 ppm remains debated, with previous studies suggesting contributors such as hydrogen-bonded BAS,[23] residual water,[24] and hydrogen-bonded silanols.[25] Changes in hydroxyl species are further confirmed in IR spectra (Figure 3b), where the disappearance of the band at 3655 cm^{-1} attributed to Al–OH groups is noted, while the bands at 3602 cm^{-1}, 3725 cm^{-1}, and 3742 cm^{-1} corresponding to BASs, internal Si–OH groups, and external Si–OH groups, respectively, remain visible.[26] Subsequent treatment with steam and HLW at 300 °C reintroduced the peaks at 2.5, 6–9 and 12–15 ppm in ^{1}H MAS NMR spectra, along with the band at 3655 cm^{-1} in IR spectra. The peak at 2.5 ppm is attributed to Al–OH groups associated with the framework-associated Al or EFAL species,[4b,14,15,22b] while the two broad signals at 6–9 and 12–15 ppm can be assigned to BAS hydrogen bonded to Al–OH groups on Al(IV)-2.[14,15] The emergence of Al–OH groups from framework-associated Al or EFAL species further clearly demonstrates that the irreversible of framework Si–O–Al bonds in both environments. As shown in Table 2, the steam-treated samples have lower concentrations of BASs and the 4.6 ppm signal but higher concentrations of Al–OH groups, the 6–9 ppm and 12–15 ppm signals, indicative of more framework tetrahedral Al atoms being irreversibly hydrolyzed. After 12 hours of treatment, the total concentrations of all species excluding Si–OH decrease significantly, indicating that Al(IV)-1 evolve into Al species without hydroxyl groups, such as framework tri-coordinated Al species, Al^{3+}, AlO^{+}, Al_2O_3, or clusters. This is consistent with the ^{27}Al and ^{29}Si MAS NMR results above. Notably, despite significant Si atom leaching and partial Al atom removal in the HLW environment, no significant change is observed in the concentration of Si–OH groups at 1.7 and 2.0 ppm, or silanol nests at 3500 cm^{-1}. This indicates that silanol nests or hydrogen-bonded Si–OH groups generated by desilication and dealumination condense to form new Si–O–Si bonds, possibly through the direct condensation of adjacent Si–OH groups or the migration of $Si(OH)_4$ species to the silanol nest for reorganization. Zhang et al. found that, in comparison to the number of BAS, Si–O–Si bonds, framework type, and EFAL, the density of silanol defects is the most crucial factor influencing HLW tolerance, irrespective of zeolite type.[6a]

The acid properties of these zeolite samples were assessed using NH_3-TPD and Py-FTIR, as shown in Figure 3c and d, respectively. Table 3 provides acid concentrations for different samples. The two ammonium-desorption peaks at around 220 and 430 °C are typically attributed to NH_3 desorption from weak and strong acid sites, respectively.[26] The decrease in acid concentrations post-AHFS treatment is attributed to the removal of framework-associated Al or EFAL species. While the reduction in acid amounts and strength decreases following steam and HLW treatment at 300 °C is a consequence of dealumination, with the severity of dealumination directly correlating with the extent of reduction. Additionally, the ratio of Brønsted to Lewis (B/L) acid concentrations was determined via pyridine adsorption at 100 °C, with their concentrations calculated from the total acid concentration measured by NH_3-TPD, as detailed in Table 3. The band at 1545 cm^{-1} corresponds to the chemisorption of pyridine to the Brønsted acid sites, while the band at 1455 cm^{-1} indicates the interaction of pyridine with Lewis acid sites.[27] As the treatment time in the HLW environment extended from 4 to 12 hours, the concentration of Brønsted acid gradually decreased, while that of Lewis acid increased, leading to a corresponding decrease in the B/L ratio. This suggests a conversion of Brønsted acid to Lewis acid. This trend was even more pronounced after steam treatment. Notably, despite treatment with AHFS solution, a residual amount of 0.076 mmol/g of Lewis acid persists, likely derived from framework tri-coordinate Al species lacking Al–OH groups, i.e. $Al(OSi)_3$.[28]

Spatial Proximity of Various Hydroxyl Species

To gain deeper insights into the spatial proximity among various hydroxyl groups after AHFS, steam, and HLW treatments, 2D ^{1}H-^{1}H DQ-SQ MAS NMR experiments were conducted. This technique provides spatial proximity information or interactions between hydroxyl groups with proton-proton distances of less than 5 Å in various zeolites, such as HZSM-5, HSSZ-13, HMOR, and HY.[8c,9a,b] Peaks appearing along the diagonal represent the autocorrelation peaks (ω, 2ω) resulting from the dipolar interaction of protons with the same chemical environment, while paired peaks appearing off-diagonal at (ω_a, $\omega_a+\omega_b$) and (ω_b, $\omega_a+\omega_b$) represent the correlations between protons with different chemical shifts. In the HZSM-5 sample (Figure 4a), intricate spatial proximity among various hydroxyl groups are observed due to diverse Al species and a low Si/Al

Table 3. Acidity characterization from NH_3-TPD and Py-IR, in units of mmol/g.

Samples	Weak acid[a]	Strong acid[a]	Total acid[a]	B acid[b]	L acid[b]	B/L[b]
HZSM-5	0.520	0.391	0.911	0.736	0.175	4.21
HZSM-5-A	0.296	0.296	0.592	0.516	0.076	6.79
HZSM-5-AH1	0.287	0.253	0.540	0.413	0.127	3.24
HZSM-5-AH2	0.219	0.215	0.434	0.305	0.129	2.37
HZSM-5-AS1	0.241	0.210	0.451	0.309	0.142	2.17
HZSM-5-A–S2	0.200	0.161	0.361	0.219	0.142	1.54

[a] Measured by NH_3-TPD. [b] B/L was calculated by relative intensity of Brønsted acids (1545 cm^{-1}) and Lewis acid sites (1455 cm^{-1}) from Py-IR, and the concentrations of Brønsted and Lewis acids were calculated from the total acid concentration measured by NH_3-TPD.

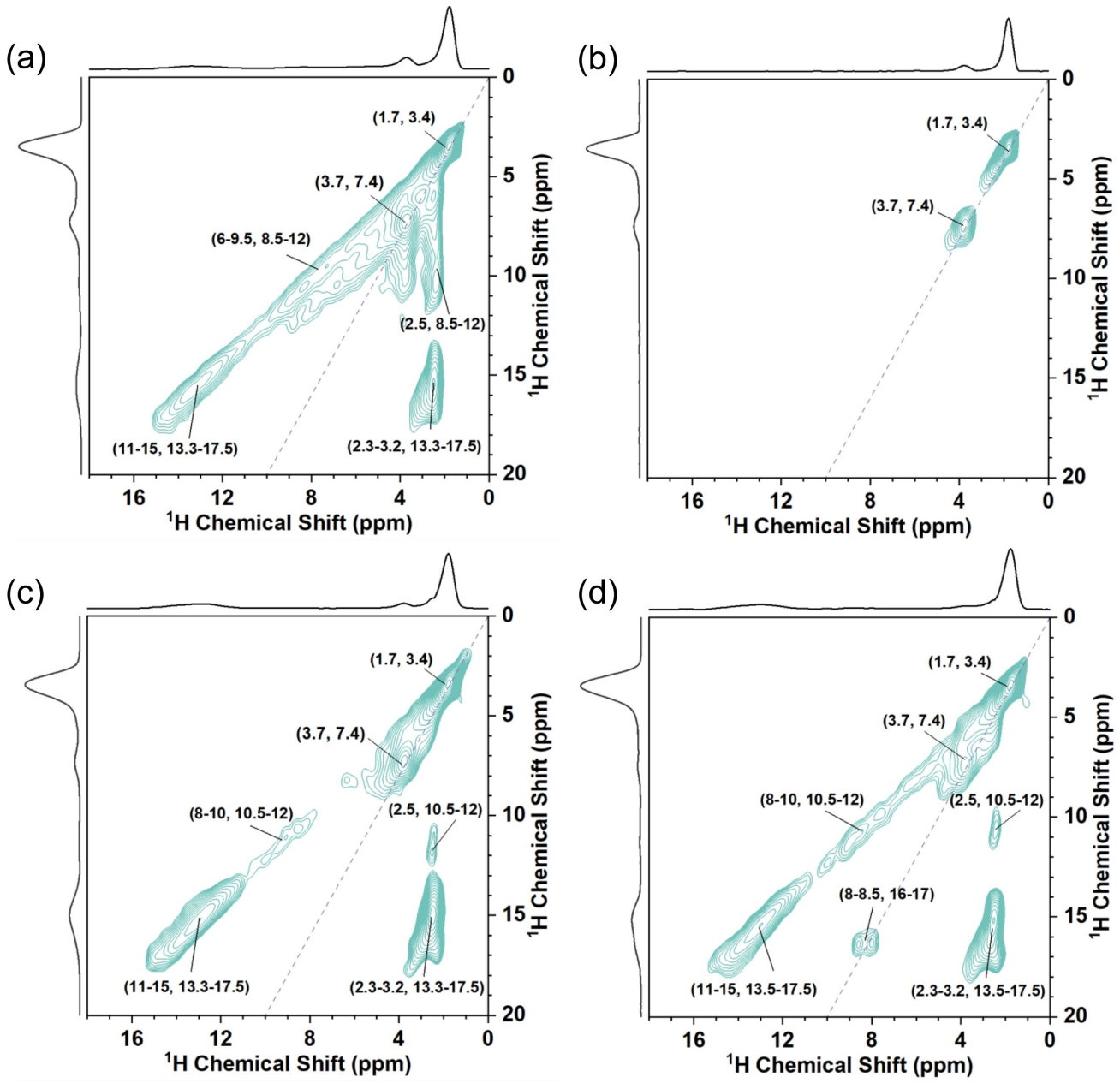

Figure 4. 2D ^{1}H-^{1}H DQ-SQ MAS NMR spectra of dehydrated HZSM-5 (a), HZSM-5-A (b), HZSM-5-AH1 (c) and HZSM-5-AS1 (d).

ratio (Si/Al = 15.7). However, for HZSM-5-A (Figure 4b), due to the disappearance of the peaks at 2.5, 6–9 and 12–15 ppm in ^{1}H MAS NMR spectra (Figure 3a), only two autocorrelation peaks at (1.7, 3.4) and (3.7, 7.4) ppm were observed. The autocorrelation peak at (1.7, 3.4) ppm corresponds to the spatial proximity between nonacidic silanol groups. Another autocorrelation peak at (3.7, 7.4) ppm suggests that bridge hydroxyl groups (Si–O(H)–Al) are not isolated but with spatial proximity. This observation was caused by the non-uniform distribution of framework Al, considering that each unit cell has 2.8 Al atoms calculated from the Si/Al of 33.7. Following steam and HLW treatment at 300 °C, the peaks at 2.5, 6–9 and 12–15 ppm were re-introduced, and the ^{1}H-^{1}H DQ MAS NMR spectrum became more complex. For HZSM-5-AH1 (Figure 4c), two new off-diagonal peak pairs at (2.5, 10.5–12.5) and (8–10, 10.5–12.5), as well as (2.3–3.2, 13.3–17.5) and (11–15, 13.3–17.5), were observed, indicating the spatial proximity between Al–OH groups and hydrogen-bonded BAS of Al(IV)-2. The spectrum of HZSM-5-AS1 sample (Figure 4d) closely resembles that of the former. A newly emerged weak autocorrelation peak at (8.0–8.5, 16–17) ppm corresponds to the spatial proximity of hydrogen-bonded BAS of Al(IV)-2, resulting from more severe dealumination caused by steam. The spatial proximity of newly generated hydroxyl groups after HLW and steam treatment shows no significant difference.

Conclusions

Overall, the structural and acidity changes of AHFS-treated HZSM-5 zeolite under steam and HLW environments was investigated using XRD, ICP, IR, NH_3-TPD, N_2 adsorption-desorption in combination with 1D&2D ssNMR spectroscopy. The evolution of framework tetrahedral Al and Si atoms in the two environments showed both similarities and differences. In the HLW environment, Si–O–Si bonds exhibit poorer hydrothermal stability than Si–O–Al bonds and result in larger pores, in contrast to the steam environment, as shown in Figure 5. Significant Si atom leaching occurs regardless of whether the framework tetrahedral Al atoms (Al(IV)-1) are removed. The evolution of Al(IV)-1 is similar to that in steam; Al(IV)-1 sequentially evolves into Al(IV)-2 and then into EFAL species through partial and complete hydrolysis. EFAL species generated in both environments act as Lewis acid sites but may have different local structures or chemical environments. Additionally, the spatial proximity of newly generated hydroxyl groups after HLW and steam treatment exhibits remarkable similarity. These findings enhance our understanding of changes in catalytic active sites and framework structure in zeolite-based catalytic processes under both in vapor-phase and aqueous conditions at the atomic scale.

Experimental Section

AHFS Treatment

The ZSM-5 zeolite catalyst (Si/Al = 12) used in this work was purchased from the Catalyst Plant of Nankai University, Tianjin, P. R. China. The NH_4-ZSM-5 zeolite was prepared via a three-fold ion-exchange of Na-ZSM-5 zeolite at 353 K in a 1.0 M aqueous solution of NH_4NO_3. To obtain HZSM-5 zeolite, calcination at 550 °C for six hours was conducted to remove organic template. The resulting HZSM-5 zeolite was washed with ammonium hexafluorosilicate (AHFS) to completely remove Al(IV)-2 and EFAL. Subsequently, HZSM-5 zeolite was dispersed in deionized water at a concentration of 30 g/L, corresponding to an AHFS:Al ratio of 2. The mixture was heated and stirred at 90 °C for 2 hours. Afterward, the mixture was centrifuged and washed three times with deionized water. This procedure was repeated three times, followed by drying overnight at 100 °C. Finally, the resulting sample, denoted as HZSM-5-A, was obtained through deammonization under vacuum ($<10^{-3}$ Pa) at 550 °C for over 15 h in a dry quartz tube.

HZSM-5-A Zeolites Steam and HLW Treatment

The schematic diagrams of the hot liquid water and steam treatments are shown in Figure S6. The detailed procedure for treating HZSM-5-A zeolite with steam and hot liquid water (HLW) is as follows: For steam treatment, 0.4 mL of deionized water and an unsealed quartz tube containing 300 mg of dehydrated HZSM-5-A zeolite were placed into a 60 mL stainless autoclave, which was then sealed in a glovebox under a dry argon (Ar) atmosphere. The autoclave was heated in a muffle furnace at 300 °C for 4 or 12 hours under a water vapor pressure of approximately 1.76 MPa. The steam-treated samples were named HZSM-5-AS1 and HZSM-5-AS2, respectively. For HLW treatment, similar to the steam treatment, the deionized water was increased to 40 mL. The autoclave was then heated in a muffle furnace at 200 °C for 12 hours under a water vapor pressure of approximately 1.55 MPa, and at 300 °C for 4 or 12 hours under a water vapor pressure of approximately 8.59 MPa. The HLW-treated samples were named HZSM-5-AH0, HZSM-5-AH1, and HZSM-5-AH2, respectively.

Ammonium Ion Exchange Treatment

The HLW-treated sample (HZSM-5-AH2) was dispersed in a 1 mol/L solution of ammonium nitrate (NH_4NO_3) at a concentration of 30 g/L and stirred at 80 °C for 2 hours. Subsequently, the mixture was centrifuged and washed three times with deionized water. This procedure was repeated three times, and the final sample in

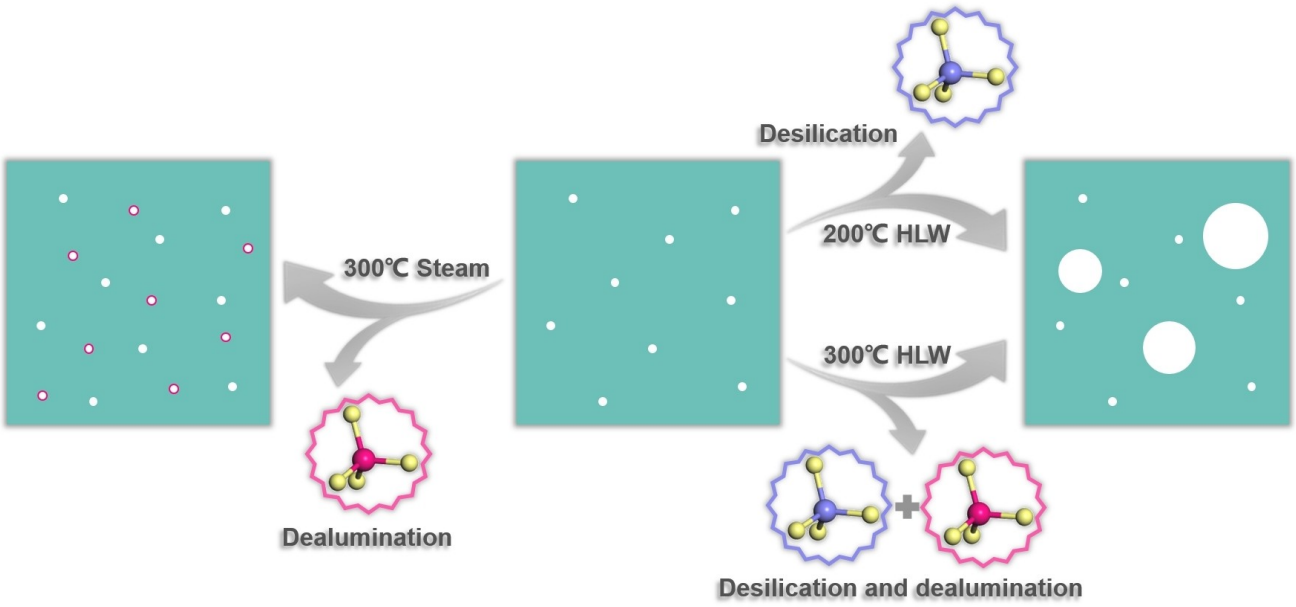

Figure 5. Diagram of evolution of HZSM-5 zeolite framework in steam and hot liquid water (HLW) environments.

ammonium form (denoted as HZSM-5-AH2-N) was dried overnight at 100 °C.

Characterization

Powder X-ray diffraction (XRD) patterns were recorded on a PANalytical X'Pert PRO X-ray diffractometer with Cu Kα radiation (λ = 1.5418 Å, 40 kV, 40 mA) to confirm the MFI-type topology structure of the samples. The crystal morphology and particle size of the samples were characterized by field emission scanning electron microscopy (FE-SEM, Hitachi, TM3000). The chemical compositions of the samples and the content of Al and Si in supernatant after HLW treatment were measured on an Inductively Coupled Plasma Optical Emission Spectrometer (ICP-OES). N_2 adsorption-desorption experiments were conducted at 77 K using a Micromeritics ASAP 2020 instrument to obtain information about the pore structure. The temperature programmed desorption of ammonia (NH_3-TPD) was carried out with Micromeritics Autochem II 2920 analyzer. 100 mg samples were outgassed at 550 °C for 1 hour under helium flow, then cooled to 100 °C and exposed to NH_3 to saturate the adsorption. The desorption process was carried out from 100 to 650 °C. Fourier transform infrared (FTIR) spectra of pyridine (Py-FTIR) analysis were recorded using a Nicolet IS50 FTIR spectrometer. The samples (about 5 mg) were pressed into a self-supporting wafer and placed into a quartz cell. The samples were pretreated at 300 °C for 1 hour under vacuum. The spectra of the pretreated samples, without pyridine absorption, were recorded from 4000 to 1000 cm^{-1}. Subsequently, the samples were cooled to 100 °C, and pyridine was introduced into the cell to saturate the adsorption. After a 30-minute evacuation of the IR cell to remove physisorbed pyridine, the spectra were recorded again. The samples were then heated to 300 °C for 30 minutes to remove weakly chemisorbed pyridine, and the spectra were recorded once more.

^{1}H, ^{27}Al and ^{29}Si MAS NMR experiments were collected on a Bruker Avance NEO 500 spectrometer operating at 11.7 T with a 3.2 mm H/F–X-Y triple resonances MAS probe. Prior to ^{1}H MAS NMR, the samples were dehydrated under vacuum ($< 10^{-3}$ Pa) at 420 °C for over 12 h in a dry quartz tube connected to vacuum line, and then were transferred into 3.2 mm NMR rotors (tightly sealed by a Kel-F cap) under a dry argon (Ar) atmosphere in a glovebox. The chemical shift of ^{1}H NMR were referenced to adamantane at 1.74 ppm. ^{1}H MAS NMR spectra were performed with a π/2 pulse width of 3.8 μs, a recycle delay of 30 s and a spinning rate of 20 kHz. The chemical shift of ^{27}Al NMR were referenced to 1 mol/L $Al(NO_3)_3$ solution at 0 ppm. ^{27}Al MAS NMR spectra were performed with a pulse width of 0.472 us (π/18), a recycle delay of 0.5 s and a spinning rate of 20 kHz. The chemical shift of ^{29}Si NMR were referenced to kaolinite at −91.5 ppm. ^{29}Si MAS NMR spectra were performed with high-power proton decoupling using a π/4 pulse width of 2.5 μs, a recycle delay of 10 s and a spinning rate of 10 kHz. The decoupling field of 62.5 kHz was applied during the acquisition time. Two-dimensional (2D) ^{1}H-^{1}H DQ-SQ MAS NMR and ^{27}Al MQ MAS NMR experiments were collected on a Bruker Avance III 600 spectrometer operating at 14.1 T with a 3.2 mm H–X-Y triple resonances MAS probe. 2D ^{1}H-^{1}H DQ-SQ MAS NMR experiments were obtained with the POST–C7 pulse sequence. 160 scans were accumulated for each of the 80 points in t1 dimensions with an increment time of 41.67 μs, a π/2 pulse width of 3.2 μs, a recycle delay of 2 s and a spinning rate of 12 kHz. ^{27}Al MQ MAS NMR spectra were obtained using the z-filter 3QMAS pulse sequence. The pulse durations were set to 4.2 μs and 1.4 μs for the first and second pulse, and the pulse width of selective pulse was set to 15 us. 3000 or 4200 scans were accumulated for each of the 64 points in t1 dimensions with an increment time of 50 μs, a recycle delay of 0.1 s and a spinning rate of 20 kHz.

Acknowledgements

This work was supported by the National Key Research and Development Program of China (2021YFA1502600, 2022YFE0116000), the National Natural Science Foundation of China (22241801, 22372169, 22022202, 22032005, 22288101, 21972142, 21991090, 21991092, 21991093), Dalian Outstanding Young Scientist Foundation (2021RJ01).

Conflict of Interests

The authors declare no conflict of interests.

Data Availability Statement

The data that support the findings of this study are available from the corresponding author upon reasonable request.

Keywords: HZSM-5 zeolite · Steam · Hot liquid water · Dealumination · Desilication

[1] T. F. Degnan, *Top. Catal.* **2000**, *13*, 349–356.
[2] a) J. N. Chheda, G. W. Huber, J. A. Dumesic, *Angew. Chem. Int. Ed.* **2007**, *46*, 7164–7183; b) T. Ennaert, J. Van Aelst, J. Dijkmans, R. De Clercq, W. Schutyser, M. Dusselier, D. Verboekend, B. F. Sels, *Chem. Soc. Rev.* **2016**, *45*, 584–611; c) D. J. Mihalcik, C. A. Mullen, A. A. Boateng, *J. Anal. Appl. Pyrolysis* **2011**, *92*, 224–232.
[3] a) C. J. Heard, L. Grajciar, F. Uhlík, M. Shamzhy, M. Opanasenko, J. Čejka, P. Nachtigall, *Adv. Mater.* **2020**, *32*, 2003264; b) D. E. Resasco, S. P. Crossley, B. Wang, J. L. White, *Catal. Rev.* **2021**, *63*, 302–362.
[4] a) T. H. Fleisch, B. L. Meyers, G. J. Ray, J. B. Hall, C. L. Marshall, *J. Catal.* **1986**, *99*, 117–125; b) L. He, J. Li, S. Han, D. Fan, X. Li, S. Xu, Y. Wei, Z. Liu, *Chem. Synth.* **2024**, *4*, 1; c) J. Holzinger, P. Beato, L. F. Lundegaard, J. Skibsted, *J. Phys. Chem. C.* **2018**, *122*, 15595–15613; d) S. M. Maier, A. Jentys, J. A. Lercher, *J. Phys. Chem. C.* **2011**, *115*, 8005–8013.
[5] a) T. Ennaert, J. Geboers, E. Gobechiya, C. M. Courtin, M. Kurttepeli, K. Houthoofd, C. E. A. Kirschhock, P. C. M. M. Magusin, S. Bals, P. A. Jacobs, B. F. Sels, *ACS Catal.* **2015**, *5*, 754–768; b) A. K. Jamil, O. Muraza, R. Osuga, E. N. Shafei, K.-H. Choi, Z. H. Yamani, A. Somali, T. Yokoi, *J. Phys. Chem. C.* **2016**, *120*, 22918–22926; c) R. M. Ravenelle, F. Schüßler, A. D'Amico, N. Danilina, J. A. van Bokhoven, J. A. Lercher, C. W. Jones, C. Sievers, *J. Phys. Chem. C.* **2010**, *114*, 19582–19595.
[6] a) L. Zhang, K. Chen, B. Chen, J. L. White, D. E. Resasco, *J. Am. Chem. Soc.* **2015**, *137*, 11810–11819; b) S. Prodinger, H. Shi, H. Wang, M. A. Derewinski, J. A. Lercher, *Appl. Catal. B-Environ.* **2018**, *237*, 996–1002; c) S. Prodinger, M. A. Derewinski, A. Vjunov, S. D. Burton, I. Arslan, J. A. Lercher, *J. Am. Chem. Soc.* **2016**, *138*, 4408–4415; d) R. Simancas, A. Chokkalingam, S. P. Elangovan, Z. Liu, T. Sano, K. Iyoki, T. Wakihara, T. Okubo, *Chem. Sci.* **2021**, *12*, 7677–7695; e) M. Li, Y. Zhou, C. Ju, Y. Fang, *Appl. Catal. A-Gen.* **2016**, *512*, 1–8; f) P. A. Zapata, Y. Huang, M. A. Gonzalez-Borja, D. E. Resasco, *J. Catal.* **2013**, *308*, 82–97.
[7] a) A. Corma, J. Mengual, P. J. Miguel, *Appl. Catal. A-Gen.* **2012**, *421–422*, 121–134; b) T. Blasco, A. Corma, J. Martineztriguero, *J. Catal.* **2006**, *237*, 267–277; c) Q. Liu, J. A. van Bokhoven, *Chem. Soc. Rev.* **2024**, *53*, 3065–3095.
[8] a) K. Stanciakova, B. Ensing, F. Göltl, R. E. Bulo, B. M. Weckhuysen, *ACS Catal.* **2019**, *9*, 5119–5135; b) S. Malola, S. Svelle, F. L. Bleken, O. Swang, *Angew. Chem. Int. Ed.* **2012**, *51*, 652–655; c) B. Fan, D. Zhu, L. Wang, S. Xu, Y. Wei, Z. Liu, *Inorg. Chem. Front.* **2022**, *9*, 3609–3618; d) Z. Yu, A. Zheng, Q. Wang, L. Chen, J. Xu, J.-P. Amoureux, F. Deng, *Angew. Chem. Int. Ed.* **2010**, *49*, 8657–8661; e) M.-C. Silaghi, C. Chizallet, E. Petracovschi, T. Kerber, J. Sauer, P. Raybaud, *ACS Catal.* **2015**, *5*, 11–15.
[9] a) S. Li, A. Zheng, Y. Su, H. Zhang, L. Chen, J. Yang, C. Ye, F. Deng, *J. Am. Chem. Soc.* **2007**, *129*, 11161–11171; b) Z. Yu, S. Li, Q. Wang, A. Zheng, X. Jun, L. Chen, F. Deng, *J.Phys. Chem. C.* **2011**, *115*, 22320–22327; c) Z.

Wang, L. Wang, Y. Jiang, M. Hunger, J. Huang, *ACS Catal.* **2014**, *4*, 1144–1147; d) S. Zhao, W. Yang, K. D. Kim, L. Wang, Z. Wang, R. Ryoo, J. Huang, *J. Phys. Chem. C.* **2021**, *125*, 11665–11676.
[10] K. Chen, M. Abdolrahmani, S. Horstmeier, T. N. Pham, V. T. Nguyen, M. Zeets, B. Wang, S. Crossley, J. L. White, *ACS Catal.* **2019**, *9*, 6124–6136.
[11] A. Vjunov, J. L. Fulton, D. M. Camaioni, J. Z. Hu, S. D. Burton, I. Arslan, J. A. Lercher, *Chem. Mater.* **2015**, *27*, 3533–3545.
[12] A. R. Maag, G. A. Tompsett, J. Tam, C. A. Ang, G. Azimi, A. D. Carl, X. Huang, L. J. Smith, R. L. Grimm, J. Q. Bond, M. T. Timko, *Phys. Chem. Chem. Phys.* **2019**, *21*, 17880–17892.
[13] a) S. Schallmoser, T. Ikuno, M. F. Wagenhofer, R. Kolvenbach, G. L. Haller, M. Sanchez-Sanchez, J. A. Lercher, *J. Catal.* **2014**, *316*, 93–102; b) M. Abdolrahmani, K. Chen, J. L. White, *J. Phys. Chem. C.* **2018**, *122*, 15520–15528.
[14] K. Chen, S. Horstmeier, V. T. Nguyen, B. Wang, S. P. Crossley, T. Pham, Z. Gan, I. Hung, J. L. White, *J. Am. Chem. Soc.* **2020**, *142*, 7514–7523.
[15] K. Chen, Z. Gan, S. Horstmeier, J. L. White, *J. Am. Chem. Soc.* **2021**, *143*, 6669–6680.
[16] a) B. H. Wouters, T. H. Chen, P. J. Grobet, *J. Am. Chem. Soc.* **1998**, *120*, 11419–11425; b) M. Ravi, V. L. Sushkevich, J. A. van Bokhoven, *Chem.Sci.* **2021**, *12*, 4094–4103.
[17] L. H. Ong, M. Dömök, R. Olindo, A. C. van Veen, J. A. Lercher, *Microporous Mesoporous Mater.* **2012**, *164*, 9–20.
[18] E. Lippmaa, A. Samoson, M. Magi, *J. Am. Chem. Soc.* **1986**, *108*, 1730–1735.
[19] T. Demuth, J. Hafner, L. Benco, H. Toulhoat, *J. Phys. Chem. B.* **2000**, *104*, 4593–4607.
[20] S. Zeng, J. Li, N. Wang, W. Zhang, Y. Wei, Z. Liu, S. Xu, *Energy Fuel* **2021**, *35*, 12319–12328.
[21] W. L. Marshall, E. U. Franck, *J. Phys. Chem. Ref. Data* **1981**, *10*, 295–304.
[22] a) M. Hunger, S. Ernst, S. Steuernagel, J. Weitkamp, *Microporous Mater.* **1996**, *6*, 349–353; b) K. Chen, M. Abdolrhamani, E. Sheets, J. Freeman, G. Ward, J. L. White, *J. Am. Chem. Soc.* **2017**, *139*, 18698–18704.
[23] a) C. Schroeder, V. Siozios, C. Mück-Lichtenfeld, M. Hunger, M. R. Hansen, H. Koller, *Chem. Mater.* **2020**, *32*, 1564–1574; b) W. Zhang, D. Ma, X. Liu, X. Liu, X. Bao, *Chem. Commun.* **1999**, *12*,1091–1092; c) H. Windeck, F. Berger, J. Sauer, *Angew. Chem. Int. Ed.* **2023**, *62*, e202303204; d) J. L. White, L. W. Beck, J. F. Haw, *J. Am. Chem. Soc.* **1992**, *114*, 6182–6189.
[24] H. Huo, L. Peng, C. P. Grey, *J. Phys. Chem. C.* **2009**, *113*, 8211–8219.
[25] C. Schroeder, V. Siozios, M. Hunger, M. R. Hansen, H. Koller, *J. Phys. Chem. C.* **2020**, *124*, 23380–23386.
[26] J. Li, M. Liu, X. Guo, S. Zeng, S. Xu, Y. Wei, Z. Liu, C. Song, *Ind. Eng. Chem. Res.* **2018**, *57*, 15375–15384.
[27] a) C. A. Emeis, *J. Catal.* **1993**, *141*, 347–354; b) N.-Y. Topsøe, K. Pedersen, E. G. Derouane, *J. Catal.* **1981**, *70*, 41–52.
[28] a) M. Hu, C. Wang, Y. Chu, Q. Wang, S. Li, J. Xu, F. Deng, *Angew. Chem. Int. Ed.* **2022**, *61*, e202207400; b) S. Xin, Q. Wang, J. Xu, Y. Chu, P. Wang, N. Feng, G. Qi, J. Trébosc, O. Lafon, W. Fan, F. Deng, *Chem. Sci.* **2019**, *10*, 10159–10169.

Manuscript received: July 21, 2024
Revised manuscript received: August 31, 2024
Accepted manuscript online: September 1, 2024
Version of record online: ■■, ■■

RESEARCH ARTICLE

The evolution of framework tetrahedral Al and Si atoms in HZSM-5 zeolite under steam and hot liquid water (HLW) environments was investigated. In HLW, Si–O–Si bonds are less stable than Si–O–Al bonds, in contrast to steam. In both environments, the tetrahedral Al species sequentially evolve into partially coordinated framework Al species and extra-framework Al species through partial and complete hydrolysis.

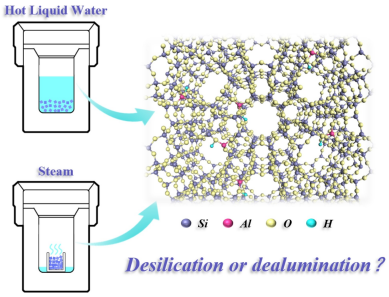

L. He, J. Niu, S. Han, D. Fan, W. Zhang, S. Xu, Y. Wei, Z. Liu*

1 – 11

Comparative Study of Si–O–Al and Si–O–Si Bond Stability in HZSM-5 Zeolite Under Steam and Hot Liquid Water Environments